Hydrodynamics in $2\frac{1}{2}$ dimensions: making jets in a plane

N Darnton[1], **O Bakajin**[1], **R Huang**[2], **B North**[1], **J O Tegenfeldt**[1] **E C Cox**[3], **J Sturm**[2] **and R H Austin**[1]

[1] Department of Physics, Princeton University, Princeton, NJ 08544, USA
[2] Department of Electrical Engineering, Princeton University, Princeton, NJ 08544, USA
[3] Department of Molecular Biology, Princeton University, Princeton, NJ 08544, USA

Abstract
We show that a careful analysis of the Navier–Stokes equation in the low Reynolds number limit has two distinct solutions, one valid for a deep, thin curtain of flow and the other for a thin wide flow. We derive a solution to the latter situation and use the results to develop a new way to control fluid flows in thin, wide sheet flow.

(Some figures in this article are in colour only in the electronic version; see `www.iop.org`)

1. Introduction: the need to control flows in $2\frac{1}{2}$D

The problems of fluid transport that are usually considered describe fluid flow in pipes, a system in which one dimension, the length, is much greater than the two other dimensions. There are, however, many occasions where one wants to control fluid flow in a sheet, a system where two of the dimensions, length and width, are much larger than the third, the height. What we call here '$2\frac{1}{2}$D hydrodynamics' describes such sheet flow. A familiar example of a $2\frac{1}{2}$D system is the flow of air that gives rise to the weather. A typical pattern of clouds shown in figure 1 arises from the turbulent flow pattern of air in the layer of atmosphere that is only at most 10 km thick which is much smaller than Earth's diameter of 30 000 km. The turbulent nature of this sheet flow makes the weather so notoriously difficult to predict. The $2\frac{1}{2}$D flows in the low-Reynolds-number world of the microfabricated chip can be predicted and controlled, particularly if some basic aspects of hydrodynamics under the unique conditions of low-Reynolds-number flow are understood.

Understanding of $2\frac{1}{2}$D flows is of great importance for the rapidly developing field of bio-device miniaturization. Over the past decade there have been immense efforts directed towards miniaturization of bio-analysis systems through applications of microfabrication. The goal is to integrate different micro-components into a single micro-total analysis system (μTAS) [1] and run an array of such systems in parallel. So far, many essential components of the μTAS have been demonstrated to perform better than their large-scale equivalents. New technologies for sorting and mixing of biomolecules [2] and for fractionation of cells from blood [3] have also arisen.
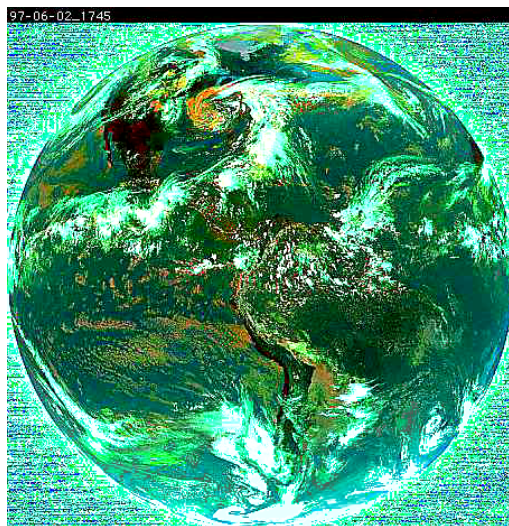
Figure 1. A snapshot from GEOS-8 of clouds over the surface of the Earth. Courtesy of NASA–Goddard Space Flight Center.

Highly integrated lab-on-a-chip devices have also been proven feasible [4–6]. For example, capillary electrophoresis (CE) on microchips has been applied to the analysis of nucleic acids, amino acids, and other types of sample [7]. Other microfabricated electrophoretic devices, such as entropic trap arrays [8], could utilize new mechanisms to enable faster fractionation of macromolecules with better resolution than conventional gel electrophoresis. Various types of microfluidic pump [9, 10] which can potentially be used to transfer samples on microchips have also been demonstrated. Many other applications, such as polymerase chain reaction (PCR) [11, 12] and fluorescence-activated cell sorting (FACS) [13, 14], have been performed on microchips. Microfabrication is the method of choice for integration of all these miniaturized components into a micro-total analysis system. Since microfabrication is basically a set of planar processes applied to planar substrates, the fluid flows in microfabricated devices are often effectively two dimensional. The thickness of the fluid flow sheet, however, cannot be ignored. The flow in these systems is NOT uniform and unbounded in the x–y plane. The z-dimension, although small compared to the characteristic sizes of the x–y plane, cannot be set to zero. In this paper we refer to such geometries (shown in figure 2) as '$2\frac{1}{2}$' dimensional.
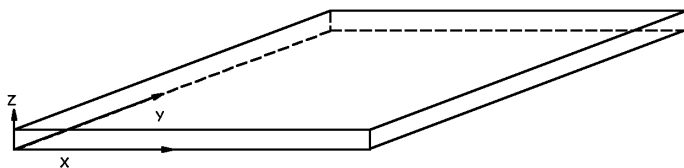

Figure 2. The x, y, z coordinate system considered for the rest of this paper. The etch depth h in the z-direction is considerably smaller than any confining boundaries in the x–y plane.

In a previous paper we explored the basic aspects of fluid flow in these structures [15], but did not explicitly consider the boundary value problems in the x–y plane. Here we show that by applying a possibly complicated set of boundary values in the x–y plane we can

properly model and control flows in planar microfabricated structures. We also show that the hydrodynamic impedance change in moving from one set of confining structures to another greatly influences the streamlines of the flow pattern in somewhat non-intuitive ways. We consider how understanding of hydrodynamics in $2\frac{1}{2}$D can help us form a thin stream of one liquid imbedded in another liquid, that we refer to as an 'injector jet'. Finally we extend these ideas to possibilities of precisely controlled complex flow patterns in microfabricated fluidic devices.

2. Somewhat simple hydrodynamics in $2\frac{1}{2}$ dimensions

In the derivation of the Navier–Stokes equation, Newton's law is of course the starting point. We consider $\boldsymbol{F} = m\boldsymbol{a}$ for a small element of fluid of mass $\mathrm{d}m = \rho\,\mathrm{d}x\,\mathrm{d}y\,\mathrm{d}z$ under the influence of a force. Since when using Newton's law one always has to follow the motion of the same atoms, the elemental boundaries $\mathrm{d}x$, $\mathrm{d}y$, and $\mathrm{d}z$ enclosing the mass $\mathrm{d}m$ change as the tubing twists and it turns out that in order to find the true acceleration one has to worry about the spatial derivatives as well as the simple $\partial v/\partial t$. This transforms the simple total derivative into a convective derivative and in the end the acceleration $\boldsymbol{a}$ is broken into two terms. Some careful thought, beautifully described in Feynman's lectures [16], then yields the famous Navier–Stokes equation that describes the movement of a viscous fluid of density ρ and viscosity η:

$$-\boldsymbol{\nabla} P + \eta\,\nabla^2 \boldsymbol{v} = \rho\left(\frac{\partial \boldsymbol{v}}{\partial t} + (\boldsymbol{v}\cdot\boldsymbol{\nabla})\boldsymbol{v}\right). \tag{1}$$

The above equation says that the forces per unit volume due to a pressure gradient ($\boldsymbol{\nabla} P$) and shear ($\eta\,\nabla^2 \boldsymbol{v}$) are equal to the mass per unit volume (ρ) times the acceleration of the fluid. The right-hand-side terms are sometimes referred to as the 'inertial forces', although they are not forces in the strict physics use of the word. If there are additional forces acting on the fluid (for instance, gravity), these terms are just added onto the left-hand side ($\rho\boldsymbol{g}$). The Navier–Stokes equation is a non-linear equation in velocity v which makes it analytically unsolvable in a general case. However, when appropriate approximations are made, the Navier–Stokes equation can be reduced and solved.

A useful concept in fluid dynamics is the ratio of the inertial forces (the right-hand side of equation (1)) to the viscous forces for steady flow because it determines what terms of the Navier–Stokes equation can be ignored in a particular situation. In steady flow, the velocity is independent of time, so $\partial v/\partial t = 0$. The magnitude of the inertial forces expressed in the term $\rho(\boldsymbol{v}\cdot\boldsymbol{\nabla})\boldsymbol{v}$ is $\rho v^2/l$, where l is a typical length scale over which the velocity changes, i.e., it is the effective size of the spatial derivative $\mathrm{d}\boldsymbol{r}$ in the Navier–Stokes equation. The viscous force, $\eta\,\nabla^2 \boldsymbol{v}$, goes as $\eta v/l^2$. This ratio, referred to as the Reynolds number, is usually written as

$$R_e = \frac{\rho l v}{\eta}. \tag{2}$$

In the microfabricated world that we are interested in, with water as the transporting fluid, the typical dimensions of the system set some limits to R_e and allow us to significantly reduce the Navier–Stokes equation. The length over which velocity changes, l, is at most 0.01 cm, the density ρ is 1 g cm^{-3}, and the viscosity η is 0.01 g cm^{-1} s^{-1}. Hence, R_e is less than 1 for fluid velocities less than 100 cm s^{-1}, a huge velocity on a chip. Since R_e in the chip is low, we can safely drop the non-linear inertial term $\rho(\boldsymbol{v}\cdot\boldsymbol{\nabla})\boldsymbol{v}$ from equation (1). In addition, we are interested in the steady-state flow with no time dependence of the velocity fields ($\partial v/\partial t = 0$). The vector equation that describes our system is then

$$\eta\,\nabla^2 \boldsymbol{v} = \boldsymbol{\nabla} P. \tag{3}$$

The second equation that our system obeys follows directly from the incompressibility of water. At the modest pressures and flows found in the world of microfabricated chips the compressibility of water is negligible. Therefore, all solutions to equation (3) will also be divergence free:

$$\nabla \cdot v = 0. \tag{4}$$

The type of flow encountered in microfabricated structures has certain unintuitive characteristics. It is known by various names: 'Stokes flow', 'creeping flow', 'potential flow', or most simply and clearly 'low-Reynolds-number flow'. At low R_e the fluid flow is determined entirely by the pressure distribution and, of course, the boundary conditions ($v = 0$ at the walls). The boundaries of a flow chamber have a profound effect on the flow profile. Such effects determine the relationship between pressure gradients and volumetric flow rates, the uniformity of velocity profiles transverse to the mean flow direction, as well as aspects of advection-enhanced diffusion (that is, enhancement of mixing by shearing flow—Taylor diffusion). Note also that equation (3) contains no time derivatives, unlike the general case of the Navier–Stokes equation (1). Because of this, under low-Reynolds-number conditions *all motion is symmetric in time*, meaning that if the pressures or forces exerted on the fluid are reversed, the motion in the fluid is completely reversed [17]. While at high Reynolds number, it is virtually impossible to move a fluid and then return it to its original state, at low Reynolds numbers (<1) this is easily done.

We start solving the Navier–Stokes equation by considering the most important physical situation encountered: the flow through a long channel. Surprising predictions for the flow profile in this case are easy to obtain. For both pipe (cylindrical) and channel (rectangular) flow, we consider a conduit of infinite extent in the z-direction, with a (fixed) pressure gradient:

$$\frac{\partial P}{\partial z} = -G \tag{5}$$

with $G > 0$. The velocity field is $v(x, y) = u(x, y)\hat{e}_z$, and is automatically divergence free for any scalar function $u(x, y)$. In the case of flow through a cylindrical pipe, the azimuthal symmetry yields

$$\frac{1}{r} \frac{\partial}{\partial r}\left(r \frac{\partial u}{\partial r}\right) = -\frac{G}{\eta} \tag{6}$$

with the boundary condition $u(R) = 0$. The solution is

$$u(r) = \frac{G}{4\eta}(R^2 - r^2). \tag{7}$$

This is the usual parabolic flow profile. It is of great interest to note that the flow is proportional simply to the gradient in the pressure with distance. Thus, we can find a very simple relationship between the total rate of fluid flow Q from a pipe of length L and the pressure drop δP across the pipe:

$$ZQ = \delta P \qquad Z = \frac{8\eta L}{\pi R^4}. \tag{8}$$

This is nothing more than Ohm's law. Ohm's law is simply the flow of electrons at low R_e!

Although we derived this simple proportionality between flow and pressure using the special case of an infinitely long cylindrical pipe at low Reynolds number, the relationship holds for any long conduit of any cross section, and even up to moderate Reynolds numbers. This original discovery that $Q \propto \delta P$ dates back to Henry Darcy's experiments with sand traps in the 1850s [18]. Provided the Navier–Stokes equation (1) can be reduced to a *linear* form, we will always find that $\delta P \propto v$, and of course $Q \propto v$ as well. The pesky non-linearity on the

right-hand side of (1) is caused by curving flows. When confined to a long, straight channel in the $\hat{z}$-direction, any fluid will eventually achieve a uniform flow with $v(x, y) = u(x, y)\hat{e}_z$. The non-linear term in the Navier–Stokes equation $(\nabla \cdot v)v = (\partial u/\partial z)v$ vanishes because u does not depend on z. With the non-linear term removed, we will always find that $A \propto \delta P$. At intermediate Reynolds numbers ($R_e > 1$, but still laminar flow), the flow entering the mouth of a pipe will take longer to settle into a steady state. This simply means that we must expand the definition of a 'long' pipe to allow a greater region at the entrance and exit of the pipe where transients will produce a deviation from the linear law. The hydrodynamic circuits at low R_e can, therefore, be modelled by simple resistive networks. This gives us a huge computational advantage over those poor souls trying to predict the weather.

So far we have solved a 1D flow problem in the pipe and we are now going to discuss flows in systems that are wide and shallow. We found that the flow in a pipe is a linear function of the pressure drop across the pipe. Much of what we want do using microfabricated chips, however, involves large 2D areas (figure 2) rather than narrow pipes. What happens when a pipe injects fluid into a large area? You might be tempted to think that in the case of laminar flow a 'jet' of fluid injected into the area would continue onwards into the area as a well-defined 'jet stream'. That is actually the case in a high-R_e situation where the inertial terms dominate. In low-R_e situations the viscous damping terms dominate and fight against any high-shear environment. Consequently the jet 'instantly' slows down to the average rate of flow in the new area. Due to the conservation of mass, it then broadens enormously.

We now make a subtle step by moving from truly three-dimensional flow to flow in a wide area in the x–y plane which is thin along the z-axis. In this wide area we assume that the thickness of the area h is much smaller than the lateral dimensions h_x and h_y (figure 2). We hope that we can separate variables by writing $v(x, y, z) = u(x, y)f(z)$. By considering the flow profile in the thin dimension z, we move from a case in 2D in which the flow would be *infinitely* deep to the $2\frac{1}{2}$D case in which the flow is shallow. Since the sheet flow is much thinner than it is wide or long, the most important boundary condition is the stick condition at the top and bottom surface. It is the shear forces against these surfaces which restrict how fast the fluid can move. The sides that are a thousand times further away than the top and bottom control the direction in which the fluid moves. The stick boundary conditions on the top and bottom surface thus will dominate and set up a standard parabolic profile:

$$f(z) = 1 - (2z/h)^2 \tag{9}$$

where h is the depth of the chip: 7 μm in the chip used below. This is sometimes known as the Darcy approximation [18]. Substitution of this form for v into equation (3) gives

$$\nabla^2 u(x, y) f(z) + \frac{2}{h^2} u(x, y) = \nabla P(x, y) \tag{10}$$

where ∇^2 now refers *only* to the dimensions x and y. Note that you can get the same equation by making the approximation

$$\frac{\partial^2}{\partial z^2} \gg \frac{\partial^2}{\partial x^2}, \frac{\partial^2}{\partial y^2} \tag{11}$$

directly in equation (3), separating variables, deducing the parabolic form for the z-dependence, and eliminating the z-coordinate.

Given that u has to be divergence free, it is convenient to define the scalar stream function $\Psi(x, y)$ which allows us to simplify the equation that we need to solve for a shallow chip even further and end up with a simple Laplace's equation. The stream function is defined such that $u \equiv \nabla \times (\Psi\hat{e}_z)$. By taking the curl of equation (10) and substituting this form of $\Psi(x, y)$,

after some vector identities we obtain

$$\left(f(z)\,\nabla^2 + \frac{2}{h^2} \right)\nabla^2 \Psi = 0. \tag{12}$$

Considering that the entire z-dependence of the problem has already been absorbed into the statement (9), the Laplace operator in equation (12) only applies to the x- and y-dimensions. The statement $\nabla^2 \ll 2/h^2$ follows as long as the boundaries in x and y are far away compared to h. The governing equation is then simply

$$\nabla^2 \Psi = 0. \tag{13}$$

This is a pleasure to solve using your favourite computer program, Fourier analysis, or conformal mapping technique.

By assuming that the Laplace's equation is valid we make some major approximations and we need to consider their consequences. If we have 'sharp' turns in the jet (near a right-angle turn or an inlet, for instance), then the equivalent assumptions (9) and (11) will fail. We expect that there will be a region of size about h in which equation (13) will not be valid. However, for most places in a large array the solution should be applicable.

Since the end result is a well-behaved two-dimensional stream function $\Psi(x, y)$, it is tempting to posit such a form from the beginning, apply the same definition $v \equiv \nabla \times (\Psi \hat{e}_z)$, substitute this into the Navier–Stokes equation, and perform the standard vector calculus manipulations. This quickly yields the biharmonic equation $\nabla^4 \Psi = 0$. Comparison with equation (12) reveals that this corresponds to the limit of *large h*: a very deep chip. This problem occurs if one specializes to a 2D stream function without imposing parabolic velocity profiles. By dropping the third dimension from the start, nothing is allowed to vary with z. In particular, all the pressures and velocities are then set to be invariant in z which is not the case in a shallow device. The case described by the biharmonic equation actually describes an *infinitely deep* chip. In fact, one of us (RHA) had a student write an entire Senior Thesis at Princeton using the biharmonic solution, and it was a dead-wrong thing to do because in fact we are in the $2\frac{1}{2}$D limit, not the 2.0 D limit. This work arose from studying ultra-fast mixing of vertical sheets of moving fluids [20] and was maybe of some utility in the case where the fluid jet is very thick [21] but not for the case of a large flat array.

For the (fourth-order) biharmonic equation (equation (12)), we must specify four boundary conditions (per dimension) to get a unique solution. The physical constraints are the no-slip conditions $v = 0$ at the boundary wall ∂D. Since $v = \nabla \times \phi \hat{z}$, we naturally impose the no-slip condition by making $\nabla\phi|_{\partial D} = 0$. This is easier to write as $\nabla\phi \cdot \hat{n} = 0$ and $\nabla\phi \times \hat{n} = 0$, where $\hat{n}$ is the unit normal to the boundary. If we impose this condition everywhere, we get the very simple solution $\phi = \text{constant}$, which correctly predicts that a completely enclosed body of fluid does not move. When we add an inflow channel we construct the long-channel flow solution and convert it to a stream function. We then impose such a ϕ on the bit of ∂D where we want fluid to flow in. For a boundary along the x-axis, the relevant stream functions could be $\phi = x - x^3/3$, $-1 \leqslant x \leqslant 1$ (for parabolic flow in the deep etch) or $\phi = x$ (for plug flow in the shallow etch). Since the long channel has translationally invariant flow, it must also have $\nabla\phi \cdot \hat{n} = 0$, where $\hat{n}$ points along the direction of flow. Since we already know that $\nabla\phi \times \hat{n} = 0$ on all the parts of ∂D where there is no channel flowing in or out, we can just integrate this along ∂D. This gives a ϕ which is constant between the channels, and analytically specified in the channels. We have, thus, constructed the eight boundary conditions for the biharmonic equation that determine ϕ everywhere: we know ϕ on all four walls, and we impose $\nabla\phi \cdot \hat{n} = 0$ on all four walls.

When we move to the second-order Laplace equation (equation (13)), the system is *overconstrained* and we have to give up some of the boundary conditions resulting in a solution

that is valid everywhere but in the narrow region near the walls. We have to give up either $\nabla\phi \times \hat{n} = 0$ or $\nabla\phi \cdot \hat{n} = 0$. The first of these guarantees that $v_\perp = 0$: i.e. that no fluid flows in or out through the wall. If we give this up, we will lose conservation of mass! The second guarantees $v_\parallel = 0$: i.e. the no-slip condition. If we lose the no-slip condition we allow infinite shear on the fluid at the boundary. In our argument we retain the first condition, and give up the second. This *definitely* and unavoidably violates the no-slip condition but it is just the mathematical consequence of assuming an infinitely shallow chip. For instance, an infinitely shallow, straight channel would have *perfectly* plug-like flow, with $v =$ constant right up to the wall, where it would fall discontinuously to zero, giving an infinitesimal region of infinite shear. Again, it is precisely this physically dubious region next to the wall which we know violates the approximations which got us to the Laplace equation in the first place. A full 3D model would correct the solution next to the wall, forcing $v_\parallel$ smoothly to zero. If we attempt to impose the usual boundary conditions of stick at the walls, so $v = 0 \rightarrow \nabla\Psi = 0$, we find that we get a problem which although annoying does not cause major problems. Inside a channel, we assume we have established plug flow: $v = c\hat{x} \rightarrow \Psi = cy$. At the very edge of a channel we no longer have plug flow, so v is not parabolic in z and the collapse from three dimensions to two is no longer meaningful. This situation falls under the caveat above: there will be a region of size h where Laplace's equation does not exactly apply. On the plus side, this means we should not get too concerned about the shape of Ψ near the edge of the channel, since we know that our differential equation is not really accurate there. In particular, we do not have to worry that the boundary condition $\Psi = cy$ produces an infinite shear at the wall of the channel.

The solution we propose here arises from a well-established Darcy's approximation to which we apply complex $x{-}y$ boundary conditions and then use to explicitly solve $v(x, y)$. In the Darcy approximation we assume a vector field $v(x, y)$ and a parabolic profile in z between the plates. The Laplacian potential function equation is really the Saffman–Taylor problem at zero tension (i.e., no surface interface between two different fluids) and in that sense it is a 'trivial' example of the much more difficult problems that Bensimon *et al* tackle in their beautiful article in *Review of Modern Physics* [19]. What IS new here is the application of complex $x{-}y$ boundary conditions that allows us to find the explicit $v(x, y)$ solutions using potential functions for two components of the same fluid moving at different initial speeds into a common area.

3. An attempt to make a uniform jet and why it fails

Let us now turn to a practical problem of making fluid run in a narrow stream of constant width across an open area. We will see how our understanding of '$2\frac{1}{2}$D' hydrodynamics can help us design a more uniform jet.

One might think that the structure shown in figure 3 would work. The philosophy behind this particular chip design was that the two wide side channels would squeeze the already narrow fluid flow from the centre channel and create a thin jet of fluid moving across the array. Figure 4 shows a wide spreading of the jet upon entering the open area. The problem arises because in a low-R_e configuration abrupt changes in fluid velocities are not allowed. The velocity of the fluid near the entrance changes slowly resulting in initial broadening of the jet profile. The jet ultimately narrows as determined by net fluxes but it has to spread first. The resulting profile, thus, is not a jet of uniform width over its entire length.

Simulations of the flow profile using the potential function solutions to equation (12) show how well the '$2\frac{1}{2}$D' Darcy approximation agrees with the data. Figure 4 shows a view of a

Figure 3. A three-port injector. The centre channel has a width of 10 μm and the two wide side channels have widths of 100 μm. The entire device is 7 μm deep
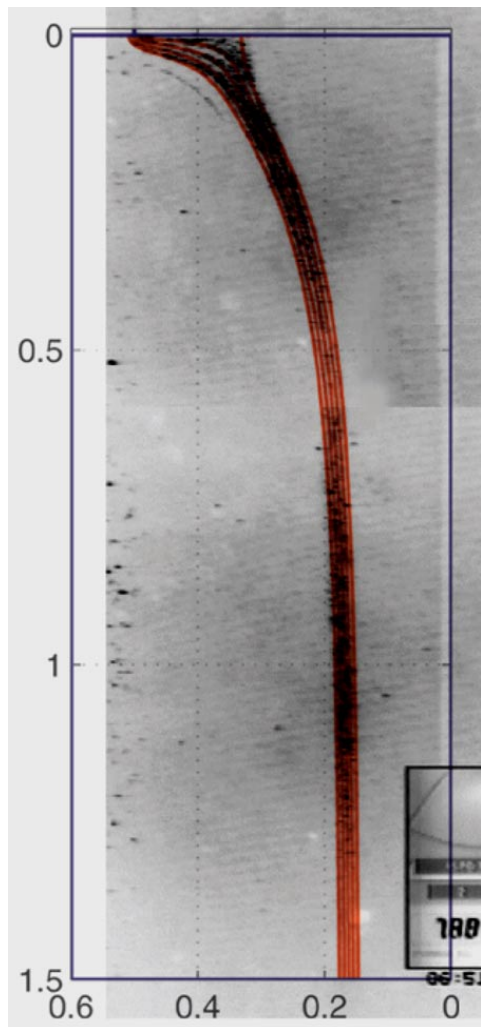

Figure 4. Comparison of data (bead tracks) and best-fit model flow lines (solid dark lines) for the fluid jet observed in a three-port jet. This figure shows the centre jet formed by higher pressure from the two side inputs. The curvature of the jet arises from the asymmetry of the position of the centre jet relative to the side jet, and the blooming of the centre jet upon entering the open area is due to the change in hydrodynamic impedance.

three-port jet with the predicted streamlines shown as dark lines and the actual flow as outlined by a stream of fluorescent balls. The Laplace solution outlined above does an excellent job of modelling these flows. Note that the solution works well even near the boundaries of the area. The simulation confirms that if there are only three channel inputs, there is always a large bulge in the initial flow pattern of the jet upon its entrance to the main open area.

4. The N-port injector idea

There is, however, a way to establish uniform and confined flow patterns by careful consideration of boundary conditions and at a cost of microfabrication complexity.

The key concept here is that the boundary values explicitly determine the flow patterns in the area and that by controlling them we can control the flow. The boundary values in hydrodynamics are determined by the fluxes of fluids at the surface. Normally, as we discussed above, we assume that the boundaries have no fluid flow across them, but this does not have to be the case. Suppose that the sides of the area have a large array of microchannels feeding a large number of streams into the area; the boundary conditions are now changed to a given flux of fluid. In principle the flux itself is an unknown quantity and difficult to posit *a priori*. However, if the fluid flux is injected into a region from a device with high fluid compliance, then the flux is constant to a high degree of accuracy and independent of the subsequent restrictions on the area into which the fluid is injected. In this way the fluid pattern becomes 'ballistic' as is true of high-R_e flow without the problems of turbulence. A high-compliance fluid source is nothing more than a current source. It can easily be constructed in a hydrodynamic array in the same way that current sources are constructed in electronics. By passing a fluid at an initial high pressure through a long narrow pipe, one ensures that most of the pressure drop occurs over the pipe and that only a small fraction of it occurs over the subsequent hydrodynamic 'circuit'. In this way the fluid flux becomes independent to first order of the low-impedance part of the circuit and the boundary conditions are fixed.

Figure 5 shows a microphotograph of a device in which the above-described principles have been applied. The large open area is an array of posts on a hexagonal lattice used for the fractionation of genomic DNA [22]. The side channels that determine the boundary value flux conditions can be seen as the series of lines feeding into the main area. These long channels act as pressure-dropping fluidic resistors and establish the current source nature of the boundary values. One of the channels is special and is connected to a unique reservoir which contains

Figure 5. A corner of an N-port array showing the array of channels feeding into an open area consisting of a hexagonal array of 2 μm posts. The width of the narrow channels feeding fluid into the array is 4 μm.

the material to be transported across the array, in our case DNA molecules. Figure 6 taken a quarter of the way down the side of the array shows the special channel, hydrodynamically isolated from the rest of the channels, which brings in the biological molecules that will be fractionated in the array. Figure 7 shows a view of this sample injection line. By properly adjusting the pressure heads on the channel reservoirs we now can inject a straight stream of fluid across a large open area without the blooming problem seen in a three-port injector shown in figure 4. Figure 8(a) and figure 8(b) show the propagation of such a flow across the hexagonal array of posts. In this example, we have a sample of DNA molecules of differing lengths transported across a wide area prior to a series of fractionating crossed field pulses [22] which again can be guaranteed to be uniform across the area because of the N-port injector current source idea.
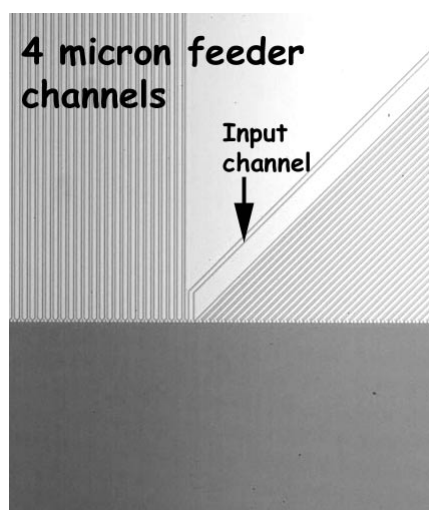

Figure 6. A view of the input channel which brings a confined stream of liquid into the array. The input channel is 6 μm wide.
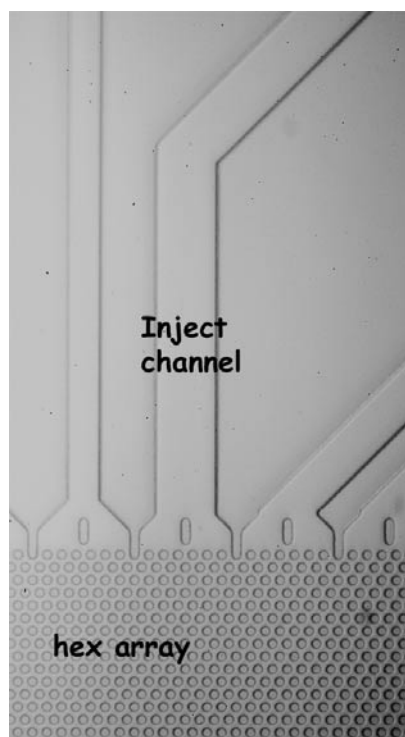
Figure 7. An enlargement of the injector channel showing the interface of the injector channel with the hexagonal array. The round posts are separated by 2 μm centre to centre.

The above-described technology can be scaled to get increasingly complex flow patterns. By having the channels divided up into a large number of independently adjustable pressure sources, the complex boundary value flux patterns can be established. The elegance of the $2\frac{1}{2}$D hydrodynamics can then be exploited to solve critical problems of transport in miniature bio-devices.
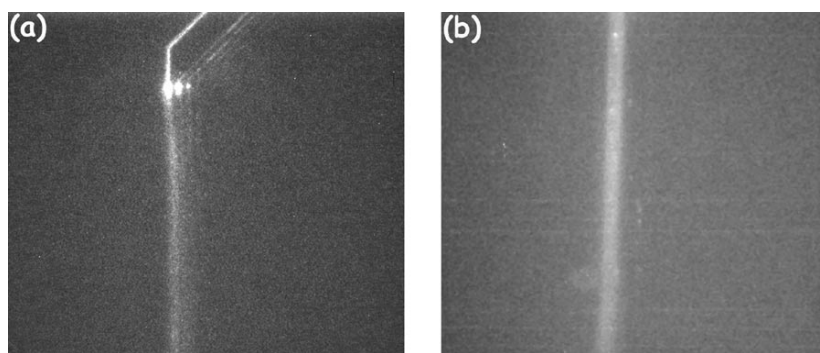
Figure 8. (a) A stream of DNA molecules injected into the post array. Some DNA molecules have been seeded into adjacent channels so that the stream lines of the injected currents can be seen. (b) The same injected jet now seen about 500 μm across the stream. The broadening seen is due to diffusion but the streamlines of the jet remain intact and focused.

Acknowledgments

References

[1] Manz A, Graber N and Widmer H M 1990 Miniaturized total chemical-analysis systems—a novel concept for chemical sensing *Sensors Actuators* B **1** 244–8

[2] Chou C-F, Austin R H, Bakajin O, Tegenfeldt J O, Castelino J A, Chan S S, Cox E C, Craighead H, Darnton N, Duke T, Han J and Turner S 2000 Sorting biomolecules with microdevices *Electrophoresis* **21** 81–90

[3] Carlson R H, Brody J P, Chan S, Gabel C, Winklemann J and Austin R H 1997 Self-sorting of white blood cells in a lattice *Phys. Rev. Lett.* **79** 2149–52

[4] Ibrahim M S, Lofts R S, Jahrling P B, Henchal E A, Weedn V W, Northrup M A and Belgrader P 1998 Real-time microchip PCR for detecting single-base differences in viral and human DNA *Anal. Chem.* **70** 2013–17

[5] Waters L C, Jacobson S C, Kroutchinina N, Khandurina J, Foote R S and Ramsey J M 1998 Microchip device for cell lysis, multiplex PCR amplification, and electrophoretic sizing *Anal. Chem.* **70** 158–62

[6] Burns M A, Johnson B N, Brahmasandra S N, Handique K, Webster J R, Krishnan M, Sammarco T S, Man P M, Jones D, Heldsinger D, Mastrangelo C H and Burke D T 1998 An integrated nanoliter DNA analysis device *Science* **282** 484–7

[7] Schmalzing D, Tsao N, Koutny L, Chisholm D, Srivastava A, Adourian A, Linton L, McEwan P, Matsudaira P and Ehrlich D 1999 Toward real-world sequencing by microdevice electrophoresis *Genome Res.* **9** 853–8

[8] Han J and Craighead H G 2000 Separation of long DNA molecules in a microfabricated entropic trap array *Science* **288** 1026–9

[9] Fuhr G, Schnelle T and Wagner B 1994 Travelling wave driven microfabricated electrohydrodynamic pumps for liquids *J. Micromech. Microeng.* **4** 217–26

[10] Lemoff A V and Lee A P 2000 An AC magnetohydrodynamic micropump *Sensors Actuators* B **63** 178–85

[11] Kopp M U, de Mello A J and Manz A 1998 Chemical amplification: continuous-flow PCR on a chip *Science* **280** 1046–8

[12] Northrup M A, Benett B, Hadley D, Landre P, Lehew S, Richards J and Stratton P A 1998 Real-time microchip PCR for detecting single-base differences in viral and human DNA *Anal. Chem.* **70** 918–20

[13] Fu A Y, Spence C, Scherer A, Arnold F H and Quake S R 1999 A microfabricated fluorescence-activated cell sorter *Nature Biotechnol.* **17** 1109–11

[14] Wolff A, Larsen U D, Blankenstein G, Philip J and Telleman P 1998 Rare event cell sorting in a microfluidic system for application in prenatal diagnosis *Micro Total Analysis Systems Proc. (Banff, Canada)* (Dordrecht: Kluwer Academic)

[15] Brody J P, Yager P, Goldstein R E and Austin R H 1996 Biotechnology at low Reynolds numbers *Biophys. J.* **71** 3430–41

[16] Feynman R, Sands M and Leighton R 1989 *The Feynman Lectures on Physics* vol 2 (Redwood City, CA: Addison-Wesley)

[17] Purcell E M 1977 Life at low Reynolds number *Am. J. Phys.* **45** 3–11

[18] Biswas A 1970 *History of Hydrology* (Amsterdam: North-Holland) pp 288–91, 308–10, 314, 319

[19] Bensimon D, Kadanoff L, Liang S, Shraiman B I and Tang C 1986 Viscous flows in two dimensions *Rev. Mod. Phys.* **58** 977–99

[20] Knight J B, Vishwanath A, Brody J P and Austin R H 1998 Hydrodynamic focusing on a silicon chip: mixing nanoliters in microseconds *Phys. Rev. Lett.* **80** 3863–6

[21] Pollack L, Tate M, Darnton N, Knight J B, Gruner S M, Eaton W A and Austin R H 1999 Compactness of the denatured state of a fast-folding protein measured by submillisecond small angle x-ray scattering *Proc. Natl Acad. Sci. USA* **96** 10 115–7

[22] Duke A J T, Austin R H, Cox E C and Chan S S 1996 Pulsed-field electrophoresis in microlithographic arrays *Electrophoresis* **17** 1075–9